1-1-2012

Graphene wrapped LiFePO4/C composites as cathode materials for Li-ion batteries with enhanced rate capability

Yi Shi
University of Wollongong, ys551@uowmail.edu.au

Shulei Chou
University of Wollongong, shulei@uow.edu.au

Jia-Zhao Wang
University of Wollongong, jiazhao@uow.edu.au

David Wexler
University of Wollongong, david_wexler@uow.edu.au

Hui-Jun Li
University of Wollongong, huijun@uow.edu.au

See next page for additional authors

Journal of Materials Chemistry

Cite this: J. Mater. Chem., 2012, 22, 16465

www.rsc.org/materials

PAPER

Graphene wrapped $LiFePO_4$/C composites as cathode materials for Li-ion batteries with enhanced rate capability

Yi Shi,[ab] Shu-Lei Chou,[b] Jia-Zhao Wang,*[b] David Wexler,[c] Hui-Jun Li,[c] Hua-Kun Liu[b] and Yuping Wu*[a]

Received 27th April 2012, Accepted 19th June 2012
DOI: 10.1039/c2jm32649c

To reduce the reaction time, electrical energy consumption, and cost, $LiFePO_4$/C/graphene has been synthesized by a rapid, one-pot, microwave-assisted hydrothermal method within 15 min at a temperature of 200 °C, followed by sintering at 600 °C for 2 h under a H_2/Ar (5 : 95, v/v) atmosphere. The microstructure and morphology of the $LiFePO_4$/C/graphene products were characterized by means of X-ray diffraction, Raman spectroscopy, field emission scanning electron microscopy, and transmission electron microscopy. The carbon coated $LiFePO_4$/C nanoparticles, around 200 nm in size, are thoroughly wrapped by crumpled micrometer-size graphene sheets. In this kind of structure, the bridging graphene nanosheets can form an effective conducting network and provide interconnected open pores that favor electrolyte absorption and reduce the diffusion path of the lithium ions. The cyclic voltammograms, charge/discharge profiles, and AC impedance measurements indicated that the kinetics of the $LiFePO_4$/C/graphene was better than that of $LiFePO_4$/C. The $LiFePO_4$/C/graphene composite exhibited a discharge capacity of 165 mA h g^{-1} at 0.1 C and 88 mA h g^{-1} at 10 C, respectively. Therefore, the $LiFePO_4$/C/graphene composite is a promising candidate for the development of high-performance, cost-effective lithium batteries for the hybrid vehicle and electric vehicle markets.

1. Introduction

$LiFePO_4$ is a very promising cathode material used in lithium ion batteries for hybrid electric vehicles (HEVs) and electric vehicles (EVs), due to its excellent thermal stability, low cost of precursors, high reversibility of Li^+ insertion/extraction, and lack of toxicity.[1] In spite of these attractive features, $LiFePO_4$ requires further modifications to overcome limitations such as poor electronic conductivity and slow lithium-ion diffusion.[2–4] Numerous approaches to solve these problems have been reported, including surface coating or admixing with electronically conductive materials,[5–7] reducing particle size and controlling morphology,[8,9] and doping with supervalent cations.[10–12] Past efforts have used various carbon sources to coat $LiFePO_4$ particles. These sources include sucrose,[13–17] poly(ethylene glycol),[17–19] citric acid,[20] and poly(vinyl alcohol).[7,21,22] Graphene, as a two-dimensional macromolecular sheet of carbon atoms with a honeycomb structure, has excellent electronic conductivity and mechanical properties, and may be the ideal conductive additive for hybrid nanostructured electrodes. Other advantages of graphene include high surface area (theoretical value of 2630 m^2 g^{-1}) for improved interfacial contact and the potential for low manufacturing costs.[23,24] Carbon coating layers and graphene in a composite can form an interparticle conductive matrix. $LiFePO_4$ nanoparticles can be connected by this network, which leads to good electronic interparticle connection.[25,26] The graphene wrapping process greatly improves the uniformity of the carbon material coating the $LiFePO_4$/C nanoparticles and provides interconnected open pores that favor electrolyte absorption and reduce the diffusion path of the lithium ions.[7,27–29]

The synthesis method for materials used in commercial HEVs and EVs should combine the advantages of simplicity, rapid synthesis, safety, and low cost. The hydrothermal route for synthesizing graphene composites is particularly successful in terms of controlling the chemical composition, particle shape, and crystallite size in a simple and inexpensive way. However, the conventional hydrothermal process involves a longer reaction time (5–12 h) to synthesize $LiFePO_4$ and produces larger submicron size particles with a wider distribution of particle size. Microwave assisted synthesis processes are appealing, as they can synthesize materials rapidly with a high degree of control of particle size and morphology and at a low cost.[30–32] Therefore, this method is more favorable for industrial manufacturing compared with the conventional hydrothermal synthesis.

This paper reports an advanced microwave-hydrothermal (MW-HT) method for preparation of $LiFePO_4$/C/graphene composites. This method has several advantages: (1) rapid

[a]New Energy and Materials Laboratory, Department of Chemistry & Shanghai Key Laboratory of Molecular Catalysis and Innovative Materials, Fudan University, Shanghai 200433, China. E-mail: wuyp@fudan.edu.cn; Fax: +86 215566 4223; Tel: +86 6564 2141
[b]Institute for Superconducting and Electronic Materials, University of Wollongong, Australia. E-mail: jiazhao@uow.edu.au; Fax: +61-2-42985731; Tel: +61-2-42981478
[c]School of Mechanical, Materials and Mechatronic Engineering, University of Wollongong, NSW 2522, Australia

synthesis of $LiFePO_4$/C/graphene by a one-pot method in 15 min; (2) synthesis of $LiFePO_4$/C/graphene at relatively low temperature and pressure; (3) microwaves can produce an *in situ* coating of wrinkled graphene on nanostructured $LiFePO_4$/C and; (4) the MW-HT method utilizes only water, as opposed to the hydrazine or sulfonate chemical reduction method which inevitably introduces non-carbon impurities into the treated composite.[5] The structure, morphology, and electrochemical properties of $LiFePO_4$/C and $LiFePO_4$/C/graphene are also presented in this paper.

2. Experimental

2.1 Materials synthesis

Graphene oxide (GO) was prepared according to the method reported by Hummers from graphite powder (Aldrich, powder, <20 μm, synthetic). $LiFePO_4$/C/graphene composite was prepared by a MW-HT synthesis process. Typically, 0.5 mg mL^{-1} GO was prepared in the form of an aqueous solution after 1 h of ultrasonic dispersion time. Appropriate quantities of $FeSO_4 \cdot 7H_2O$, Li_3PO_4, ascorbic acid, and glucose (20 wt. %), such that the weight ratio of GO to $LiFePO_4$ would be 15 : 85, were dissolved into this solution. The molar ratio of Li : Fe: P was 3 : 1 : 1. After vigorous magnetic stirring for 20 min, this solution was transferred to a 50 mL Teflon® lined autoclave. The system was operated at a frequency of 2.45 GHz and a power of 300 W, and the sample temperature was ramped to 200 °C and kept at 200 °C for 15 min under hydrothermal conditions. After the solution cooled down to room temperature, the precipitate powder was filtrated and washed several times with deionized water and acetone. Then, the obtained powder was dried at 80 °C for 4 h in a vacuum oven, followed by sintering at 600 °C for 2 h under a H_2/Ar (5 : 95, v/v) atmosphere to yield the $LiFePO_4$/C/graphene composite. As a reference, $LiFePO_4$ (without GO addition) was also prepared following the same procedure.

2.2 Material characterization

X-Ray diffraction (XRD) (GBC MMA) data were collected from powder samples at a scanning rate of 2° min^{-1} for 2θ in the range of 10–50°. Traces™ software in combination with the Joint Committee on Powder Diffraction Standards (JCPDS) powder diffraction files was used to identify the phases present. Raman analysis was performed using a Raman spectrometer (Jobin Yvon HR800) employing a 10 mW helium/neon laser at 632.8 nm. The amount of graphene in the samples was estimated using a Mettler-Toledo thermogravimetric analysis/differential scanning calorimetry (TGA/DSC) 1 Stare System from 50–800 °C at 5 °C min^{-1} in air flux. The morphologies of the samples were investigated by field emission scanning electron microscopy (FE-SEM; JEOL JSM-7500FA). Transmission electron microscopy (TEM) investigations were performed using a 200 kV JEOL 2011. TEM samples were prepared by deposition of ground particles onto holey carbon support films, with care taken to ensure that selected area electron diffraction (SAED) and high resolution TEM contrast were obtained only from sample regions located over holes in the holey carbon support films. To test the electrochemical performance, sample powders were mixed with carbon black and poly(vinylidene fluoride) (PVDF) in a weight ratio of 80 : 10 : 10, pasted on aluminum foil, and then dried in a vacuum oven at 80 °C for 8 h. CR 2032 coin-type cells were assembled in an Ar-filled glove box (Mbraun, Unilab, Germany) using lithium metal foil as the counter electrode. The electrolyte was 1 M $LiPF_6$ in a mixture of ethylene carbonate (EC) and dimethyl carbonate (DMC) (1 : 1 by volume, provided by MERCK KGaA, Germany). The cells were galvanostatically charged and discharged in the range of 4.2–2 V at different rates using a computer-controlled charger system manufactured by Land Battery Testers. Cyclic voltammetry (CV) was conducted by using a Biologic VMP3 electrochemistry workstation at a scanning rate of 0.1 mV s^{-1} between 2.0 and 4.2 V. Electrochemical impedance spectroscopy (EIS) was performed on the electrodes using a Biologic VMP3 electrochemistry workstation. The AC amplitude was 5 mV, and the frequency range applied was 100 kHz to 0.01 Hz.

3. Results and discussion

Fig. 1 shows the X-ray diffraction (XRD) patterns obtained from the $LiFePO_4$/C and $LiFePO_4$/C/graphene composites, in which the majority of diffraction lines can be indexed to the orthorhombic $LiFePO_4$ phase. Diffraction peaks which might appear for graphene or amorphous carbon are absent, most likely because they are below the limits of detection by XRD or, in the case of the graphene (002) peak, because they are likely to be eclipsed by the $LiFePO_4$ (011) peak. The absence of a reflection peak at approximately 11° indicates that the GO cannot be distinguished, consistent with full or partial reduction to graphene.

Further information on the structure of the $LiFePO_4$/C and $LiFePO_4$/C/graphene composites was obtained from the associated Raman spectra (Fig. 2). The bands at 500–100 cm^{-1} and 1120–520 cm^{-1} correspond to the Raman vibrations of Fe–O and PO_4^{3-} in $LiFePO_4$, respectively, while the bands in the range of 1200–1460 cm^{-1} and 1470–1730 cm^{-1} are attributed to the D-band (K-point phonons of A_{1g} symmetry) and G-band (E_{2g} phonons of Csp^2 atoms). The broadening of the D and G bands with a strong D line indicates localized in plane sp^2 domains and disordered graphitic crystal stacking of the graphene nanosheets. The I_D/I_G value (the peak intensity ratio between the 1325 and 1588 cm^{-1} peaks) generally provides a useful index for comparing the degree of crystallinity of various carbon materials, *i.e.*, the smaller the I_D/I_G ratio, the higher the degree of ordering in the carbon material.[5] The I_D/I_G values of graphene, and the

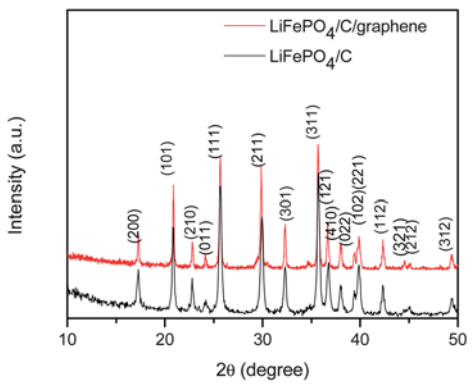

Fig. 1 XRD patterns of $LiFePO_4$/C and $LiFePO_4$/C/graphene composites.

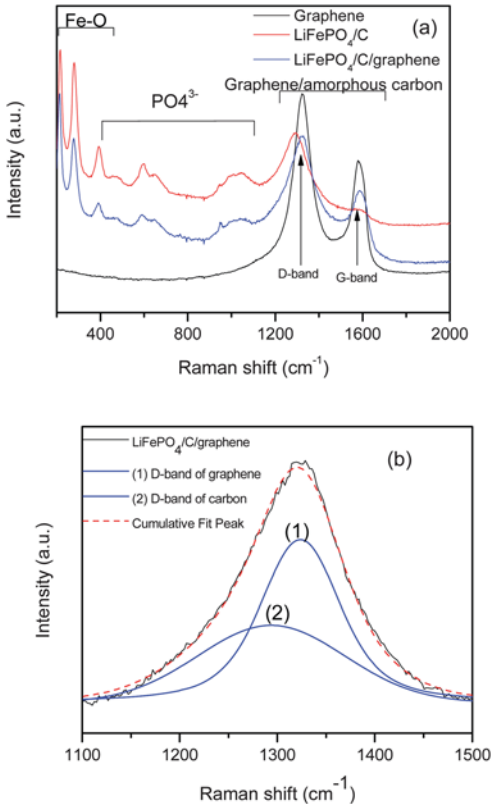

Fig. 2 (a) Raman spectra of graphene, and $LiFePO_4$/C and $LiFePO_4$/C/graphene composites. (b) Fitting results for disordered band (D-band).

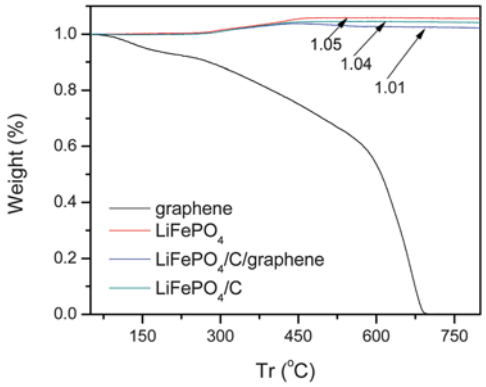

Fig. 3 TGA curves of graphene, $LiFePO_4$, and $LiFePO_4$/C and $LiFePO_4$/C/graphene composites.

$LiFePO_4$/C/graphene and $LiFePO_4$/C composites are 1.52, 1.87, and 17.31, respectively.[30] The $LiFePO_4$/C/graphene composite shows a similar I_D/I_G value to graphene. Therefore, the Raman results are consistent with the formation of $LiFePO_4$/C/graphene composites.[33]

Fig. 3 shows that the mass increase of $LiFePO_4$ is around 5% of the total weight when it is heated up to 800 °C. Theoretically, carbon components should be decomposed at such a high temperature and lead to a decrease in the total weight of the composite. The total mass increase of the $LiFeO_4$/C composite at 800 °C is about 4%, indicating that the carbon concentration should be relatively low, perhaps 1%. On the other hand, the $LiFeO_4$/C/graphene composite showed a weight change of 3% *vs.* $LiFePO_4$/C. Accordingly, the total weight percentage of the graphene can be calculated as 3% in total.

Fig. 4 displays FESEM (Fig. 4(a)) and TEM (Fig. 4(b–d)) images obtained from the $LiFePO_4$/C/grapheme composite. The average particle size of the $LiFePO_4$/C prepared by the MW-HT method is around 150 nm. Both FESEM (Fig. 4(a)) and TEM revealed that the $LiFePO_4$ nanoparticles are wrapped up in crumpled micrometer-size graphene sheets. Selected area electron diffraction of clusters of particles located over holes in the support film (Fig. 4(b) inset) revealed contrast consistent with the presence of both amorphous carbon (diffuse ring) and overlapping graphene (sharp rings). The contrast in high resolution TEM (HRTEM) images was also consistent with this, and indicated that the wrapping of individual particles was tight (Fig. 4(c) and (d)). For example, the HRTEM image in Fig. 4(d) indicates that the $LiFePO_4$ particle coated by carbon is wrapped up in more than 5 sheets of graphene. In this kind of structure, the bridging graphene nanosheets can form an effective conducting network.

At the same time, a porous network between the $LiFePO_4$/C and the graphene nanosheets was formed in the random hybrid composite, which is believed to facilitate the penetration of the electrolyte to the surface of the active materials, resulting in superior rate capability and enhanced reversible capacity in comparison with the $LiFePO_4$.[33] A schematic drawing of this is shown in Fig. 5.

The electrochemical performance of $LiFePO_4$/C and $LiFePO_4$/C/graphene composites was evaluated by cyclic voltammetry (CV) and galvanostatic charge/discharge cycling using CR 2032 coin cells.

Fig. 6 shows the cyclic voltammograms of $LiFePO_4$/C and $LiFePO_4$/C/graphene for the first five cycles. Both the $LiFePO_4$/C and the $LiFePO_4$/C/graphene electrodes show a pair of redox peaks at about 3.57 V/3.27 V, consistent with a two-phase redox reaction of $LiFePO_4 \rightarrow FePO_4 + Li^+ + e$. Careful comparison of the redox peaks shows that the peak separation exhibited by the $LiFePO_4$/C/graphene electrode is about 86 mV smaller than that exhibited by the $LiFePO_4$/C electrode. This result suggests that the $LiFePO_4$/C/graphene electrode has better kinetic properties, and we think that this phenomenon is mainly due to the graphene. A continuous increase in the cathodic peak current from the CV curves can be observed in the first five scans, as well as in the corresponding peak area. A similar observation has been reported in previous research, which has been ascribed to an activation effect during the initial cycling of the $LiFePO_4$ and carbon material composites.[34]

Fig. 7 shows the charge/discharge profiles of the $LiFePO_4$/C and $LiFePO_4$/C/graphene composites in the first cycle. The corresponding potential capacity diagram for the first cycle shows a typical flat potential plateau at 3.4 V *versus* Li/Li^+. The $LiFePO_4$/C/graphene electrode delivered a discharge capacity of 165 mA h g^{-1} (specific capacity is based on $LiFePO_4$ only) at the 0.1 C rate (10 hours charge and 10 hours discharge), which is very close to the theoretical capacity of $LiFePO_4$ (170 mA h g^{-1}), while the discharge capacity of $LiFePO_4$/C under the same conditions is only 125 mA h g^{-1}. Furthermore, the discharge curve of the $LiFePO_4$/C/graphene composite is more flattened than that of the $LiFePO_4$/C. The polarization between the charge and discharge plateaus is reduced from 158 mV to 98 mV for the

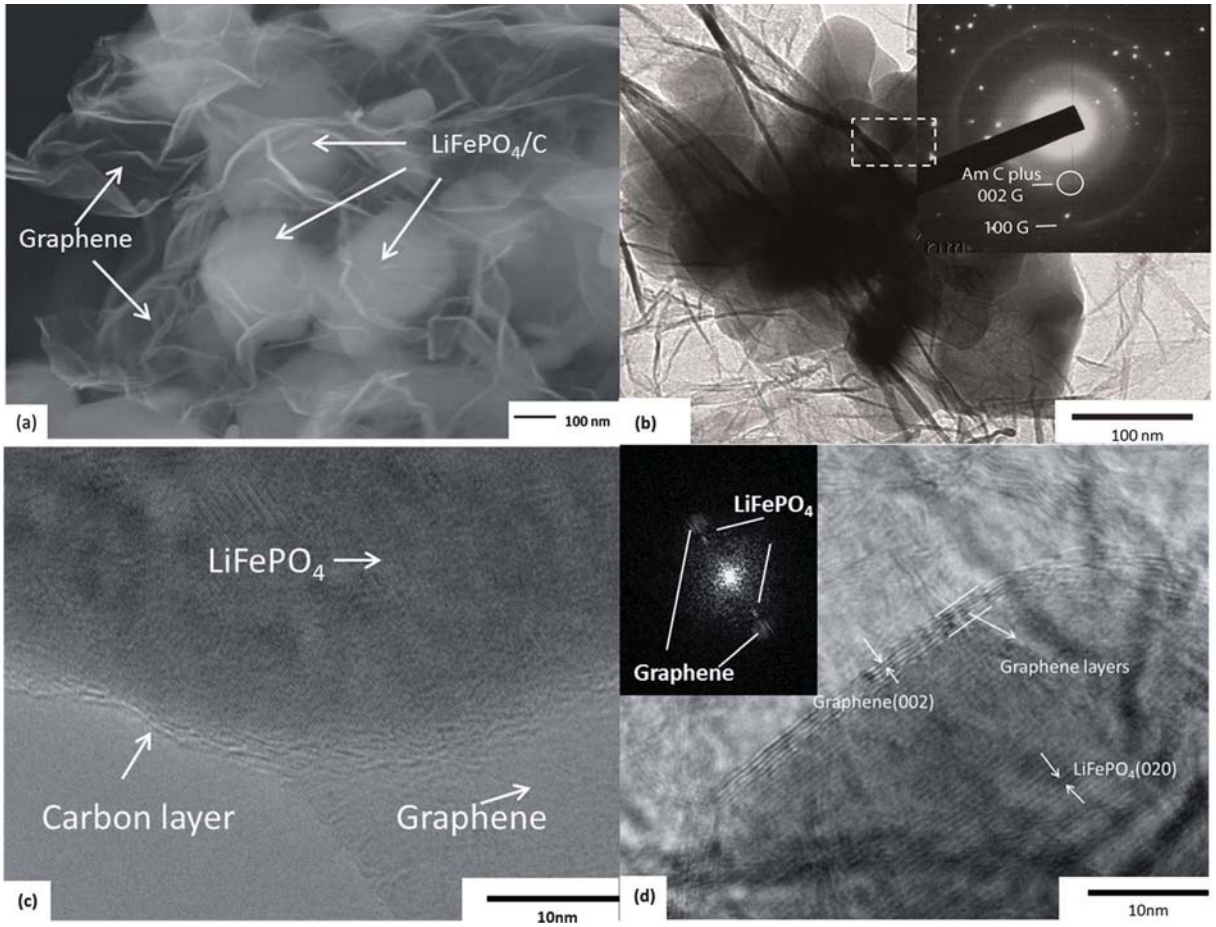

Fig. 4 FESEM and TEM images of $LiFePO_4$/C/graphene composite: (a) FESEM secondary electron image of large area, (b) TEM image and associated selected area electron diffraction pattern from $LiFePO_4$ particles wrapped in graphene nanosheets and located over a hole in the carbon support film. (c) HRTEM image of LiFePO4/C/graphene composite, (d) HRTEM image of a graphene wrapped $LiFePO_4$ particle with the inset diffractogram indicating the graphene (002) and $LiFePO_4$ (020) lattice planes.

$LiFePO_4$/C/graphene composite, indicating that the kinetics of the $LiFePO_4$/C is indeed improved by graphene addition. This is considered to be because the graphene nanosheets act as conducting routes between the $LiFePO_4$ nanoparticles, resulting in significantly reduced contact resistance.

Comparisons of the rate performance of the $LiFePO_4$/C and $LiFePO_4$/C/graphene composites are shown in Fig. 8. After the cells had been cycled for 10 cycles at a rate of C/10, the current densities were increased stepwise to 10 C. The $LiFePO_4$/C/graphene composites exhibit obviously improved electrochemical

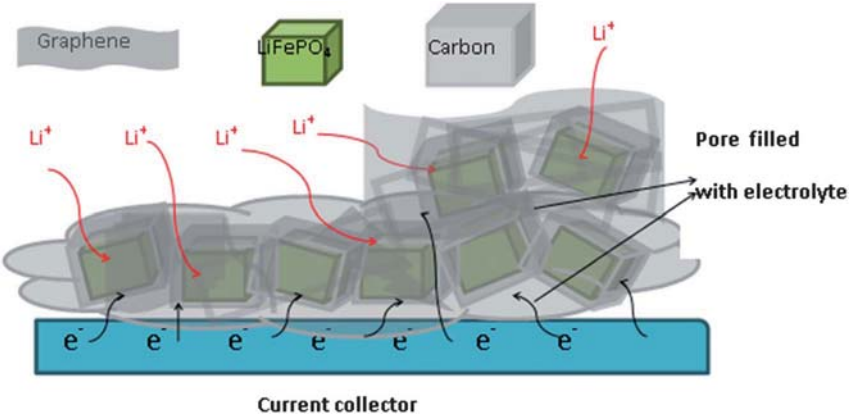

Fig. 5 Schematic diagram of the bridging graphene nanosheet/$LiFePO_4$ structure, which could be responsible for the superior properties of the $LiFePO_4$/C/graphene composite.

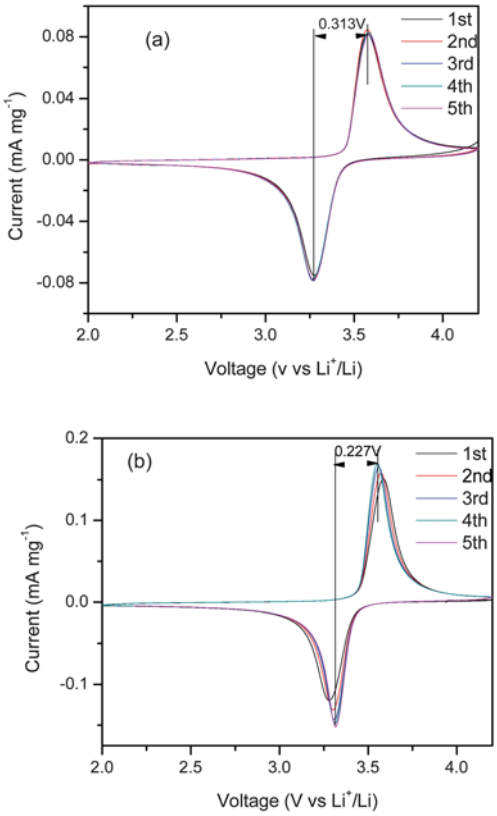

Fig. 6 Cyclic voltammograms for the first five cycles of (a) $LiFePO_4$/C at a scan rate of 0.1 mV s^{-1}, (b) $LiFePO_4$/C graphene at a scan rate of 0.1 mV s^{-1}.

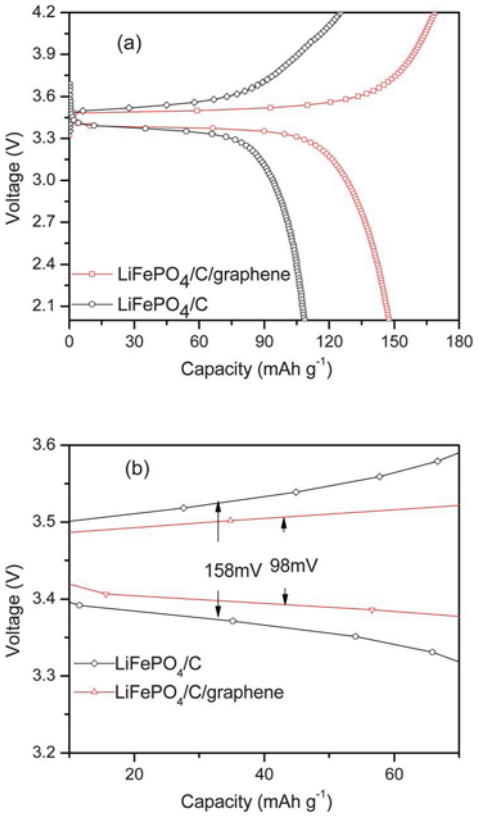

Fig. 7 (a) The first discharge and charge profile of the $LiFePO_4$/C and $LiFePO_4$/C/graphene composites at the current density of 0.1 C between the voltage limits of 2 and 4.2 V in EC/DMC solution containing 1 M $LiPF_6$. (b) Magnification of the charge/discharge plateau in Fig. 7(a).

performance. A highly stable reversible capacity of 88 mA h g^{-1} was obtained at the highest current density of 10 C, while there was only a value of 50 mA h g^{-1} for $LiFePO_4$/C. After 40 cycles under various conditions, the $LiFePO_4$/C/graphene cell delivers about 99% of the initial capacity. Fig. 8(b) shows the specific capacity as a function of rate for lithium cells containing $LiFePO_4$/C and $LiFePO_4$/C/graphene. As shown in Fig. 8(b), the capacity of $LiFePO_4$/C/graphene decreases much more slowly with increasing discharge rates than that of $LiFePO_4$/C/graphene. The cycling performance is comparable to those of reported $LiFePO_4$/graphene composites[25,27,33–35] and even better than those of $LiFePO_4$/C composites.[25,31] The rate performance and cycling stability of the $LiFePO_4$/C/graphene could be attributed to the nanosize particles with very high surface area and improved conductivity through a superior graphene conductor.

Fig. 9 shows Nyquist plots of both samples in the discharged state and the equivalent circuit that was used for interpretation (inset). EIS spectra of the $LiFePO_4$/C and $LiFePO_4$/C/graphene composite electrodes were collected after charge–discharge for five cycles at the potential of 3.4 V. The Nyquist plots (Fig. 9) show one compressed semicircle in the high to medium frequency range, which describes the charge transfer resistance (R_{ct}) for both electrodes, and an approximately 45° inclined line in the low-frequency range, which could be considered as Warburg impedance (Z_W), which is associated with the lithium-ion diffusion in the bulk of the active material. While the high-frequency intercept of the semicircle is related to the uncompensated resistance (R_u), the diameter of the semicircle is related to the charge transfer resistance (R_{ct}).[31] From comparing the diameters of the semicircles, the impedance of the $LiFePO_4$/C electrode is significantly larger than that of the $LiFePO_4$/C/graphene electrode. The values of R_{ct} for the $LiFePO_4$/C and $LiFePO_4$/C/graphene electrodes were calculated to be 513 Ω and 201 Ω, respectively. Obviously, the R_{ct} of the $LiFePO_4$/C/graphene electrode is much smaller than that of the $LiFePO_4$/C electrode, indicating the enhanced ionic conductivity of the $LiFePO_4$/C/graphene composite.

4. Conclusions

In conclusion, a highly ordered $LiFePO_4$/C/graphene nanocomposite has been developed by a rapid, facile microwave-hydrothermal route, in which $LiFePO_4$/C nanoparticles are embedded in conductive and interconnected graphene networks. This nano-architecture ensures not only intimate contact between the liquid electrolyte and the active $LiFePO_4$/C nanoparticles, but also high electronic conductivity for both facile mass transfer and facile charge transfer. The results clearly demonstrate that the $LiFePO_4$/C/graphene electrode has highly desirable properties: a specific capacity approaching the theoretical value, stable cycle life, and exceptional rate capability. Such a combination does not exist in common $LiFePO_4$ cathode materials or even in $LiFePO_4$/C. Therefore, $LiFePO_4$/C/graphene

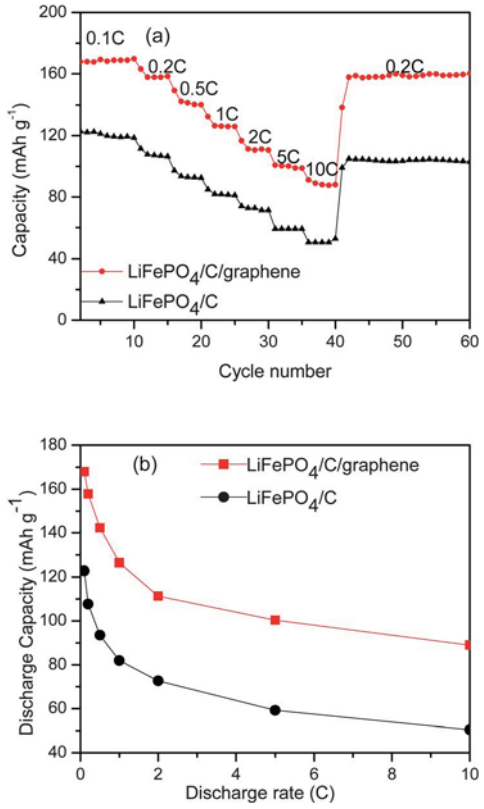

Fig. 8 (a) Rate performance of $LiFePO_4$/C and $LiFePO_4$/C/graphene composites cycled in EC/DMC solution containing 1 M $LiPF_6$. (b) Capacity *versus* discharge rate for the $LiFePO_4$/C and $LiFePO_4$/C/graphene composites.

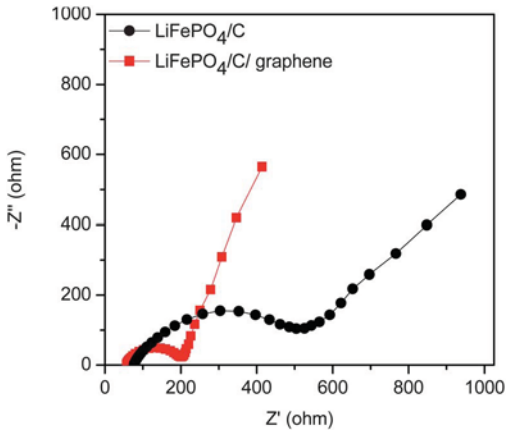

Fig. 9 Nyquist plots of $LiFePO_4$/C and $LiFePO_4$/C/graphene composite electrodes with equivalent circuit (inset).

electrode is a promising candidate for the development of high-performance, low-cost, advanced lithium batteries directed to the electric and hybrid electric vehicle markets.

Acknowledgements

Financial support was provided by an Australian Research Council (ARC) Discovery Project (DP100103909). Financial support from the National Natural Science Foundation of China (NSFC) (21073046) is also greatly appreciated. Technical assistance on the FESEM by Chao Zhong is highly appreciated. The authors acknowledge use of facilities within the UOW Electron Microscopy Centre. This research used equipment funded by Australian Research Council grant(s) and located at the UOW Electron Microscopy Centre. Many thanks also go to Dr Tania Silver for critical reading of the manuscript.

Notes and references

1 M. S. Song, Y. M. Kang, J. H. Kim, H. S. Kim, D. Y. Kim, H. S. Kwon and J. Y. Lee, *J. Power Sources*, 2007, **166**, 260.
2 F. Gao and Z. Tang, *Electrochim. Acta*, 2008, **53**, 5071.
3 X. Xia, Z. Wang and L. Chen, *Electrochem. Commun.*, 2008, **10**, 1442.
4 J. Wang and X. Sun, *Energy Environ. Sci.*, 2012, **5**, 5163.
5 X. L. Wu, L. Y. Jiang, F. F. Cao, Y. G. Guo and L. J. Wan, *Adv. Mater.*, 2009, **21**, 2710.
6 G. Wang, H. Liu, J. Liu, S. Qiao, G. M. Lu, P. Munroe and H. Ahn, *Adv. Mater.*, 2010, **22**, 4944.
7 S. W. Oh, S. T. Myung, S. M. Oh, K. H. Oh, K. Amine, B. Scrosati and Y. K. Sun, *Adv. Mater.*, 2010, **22**, 4842.
8 A. Yamada, S. C. Chung and K. Hinokuma, *J. Electrochem. Soc.*, 2001, **148**, A224.
9 M. Takahashi, S. Tobishima, K. Takei and Y. Sakurai, *J. Power Sources*, 2001, **97–98**, 508.
10 J. D. Wilcox, M. M. Doeff, M. Marcinek and R. Kostecki, *J. Electrochem. Soc.*, 2007, **154**, A389, DOI: 10.1149/1.2667591.
11 S. Y. Chung, J. T. Bloking and Y. M. Chiang, *Nat. Mater.*, 2002, **1**, 123.
12 M. S. Song, D. Y. Kim, Y. M. Kang, Y. I. Kim, J. Y. Lee and H. S. Kwon, *J. Power Sources*, 2008, **180**, 546.
13 X. Z. Liao, Z. F. Ma, L. Wang, X. M. Zhang, Y. Jiang and Y. S. He, *Electrochem. Solid-State Lett.*, 2004, **7**, A522.
14 J. Ying, M. Lei, C. Jiang, C. Wan, X. He, J. Li, L. Wang and J. Ren, *J. Power Sources*, 2006, **158**, 543.
15 C. Delmas, M. Maccario, L. Croguennec, F. Le Cras and F. Weill, *Nat. Mater.*, 2008, **7**, 665.
16 A. D. Spong, G. Vitins and J. R. Owen, *J. Electrochem. Soc.*, 2005, **152**, A2376.
17 S. Bewlay, K. Konstantinov, G. Wang, S. Dou and H. Liu, *Mater. Lett.*, 2004, **58**, 1788.
18 Z. Xu, L. Xu, Q. Lai and X. Ji, *Mater. Res. Bull.*, 2007, **42**, 883.
19 L. Wang, Z. Zhang and K. Zhang, *J. Power Sources*, 2007, **167**, 200.
20 K. F. Hsu, S. Y. Tsay and B. J. Hwang, *J. Mater. Chem.*, 2004, **14**, 2690.
21 B. Zhao, Y. Jiang, H. Zhang, H. Tao, M. Zhong and Z. Jiao, *J. Power Sources*, 2009, **189**, 462.
22 F. Gao, Z. Tang and J. Xue, *Electrochim. Acta*, 2007, **53**, 1939.
23 D. Wang, D. Choi, J. Li, Z. Yang, Z. Nie, R. Kou, D. Hu, C. Wang, L. V. Saraf and J. Zhang, *ACS Nano*, 2009, **3**, 907.
24 Y. Sun, Q. Wu and G. Shi, *Energy Environ. Sci.*, 2011, **4**, 1113.
25 Y. Zhang, H. Feng, X. Wu, L. Wang, A. Zhang, T. Xia, H. Dong and M. Liu, *Electrochim. Acta*, 2009, **54**, 3206.
26 X. Zhou, F. Wang, Y. Zhu and Z. Liu, *J. Mater. Chem.*, 2011, **21**, 3353.
27 J. Yang, J. Wang, D. Wang, X. Li, D. Geng, G. Liang, M. Gauthier, R. Li and X. Sun, *J. Power Sources*, 2012, **208**, 340.
28 Y. Wang, Z. S. Feng, J. J. Chen and C. Zhang, *Mater. Lett.*, 2012, **71**, 54.
29 Y. Tang, F. Huang, H. Bi, Z. Liu and D. Wan, *J. Power Sources*, 2012, **203**, 130.
30 A. V. Murugan, T. Muraliganth and A. Manthiram, *J. Phys. Chem. C*, 2008, **112**, 14665.
31 A. V. Murugan, T. Muraliganth and A. Manthiram, *J. Electrochem. Soc.*, 2009, **156**, A79.
32 S. L. Chou, J. Wang, H. Liu and S. X. Dou, *J. Phys. Chem. C*, 2011, **115**, 16220.
33 L. Wang, H. Wang, Z. Liu, C. Xiao, S. Dong, P. Han, Z. Zhang, X. Zhang, C. Bi and G. Cui, *Solid State Ionics*, 2010, **181**, 1685.
34 X. F. Guo, H. Zhan and Y. H. Zhou, *Solid State Ionics*, 2009, **180**, 386.
35 Y. Ding, Y. Jiang, F. Xu, J. Yin, H. Ren, Q. Zhuo, Z. Long and P. Zhang, *Electrochem. Commun.*, 2010, **12**, 10.

